REPORT DOCUMENTATION PAGE

Form Approved OMB NO. 0704-0188

1. REPORT DATE (DD-MM-YYYY)	2. REPORT TYPE	3. DATES COVERED (From - To)
25-03-2019	Final Report	15-Sep-2011 - 31-May-2015

4. TITLE AND SUBTITLE
Final Report: Charge Storage Properties of Early Transition Metal Nitrides

5a. CONTRACT NUMBER
W911NF-11-1-0465

5b. GRANT NUMBER

5c. PROGRAM ELEMENT NUMBER
611102

6. AUTHORS

5d. PROJECT NUMBER

5e. TASK NUMBER

5f. WORK UNIT NUMBER

7. PERFORMING ORGANIZATION NAMES AND ADDRESSES
University of Michigan - Ann Arbor
3003 South State Street

Ann Arbor, MI 48109 -1274

8. PERFORMING ORGANIZATION REPORT NUMBER

9. SPONSORING/MONITORING AGENCY NAME(S) AND ADDRESS (ES)
U.S. Army Research Office
P.O. Box 12211
Research Triangle Park, NC 27709-2211

10. SPONSOR/MONITOR'S ACRONYM(S)
ARO

11. SPONSOR/MONITOR'S REPORT NUMBER(S)
58456-CH.2

12. DISTRIBUTION AVAILIBILITY STATEMENT
Approved for public release; distribution is unlimited.

13. SUPPLEMENTARY NOTES
The views, opinions and/or findings contained in this report are those of the author(s) and should not contrued as an official Department of the Army position, policy or decision, unless so designated by other documentation.

14. ABSTRACT

15. SUBJECT TERMS

16. SECURITY CLASSIFICATION OF:			17. LIMITATION OF ABSTRACT	15. NUMBER OF PAGES	19a. NAME OF RESPONSIBLE PERSON
a. REPORT	b. ABSTRACT	c. THIS PAGE			Levi Thompson
UU	UU	UU	UU		19b. TELEPHONE NUMBER 734-936-2015

RPPR Final Report
as of 23-Apr-2019

Agency Code:

Proposal Number: 58456CH **Agreement Number: W911NF-11-1-0465**
INVESTIGATOR(S):

Name: Alice Eleanor Sylvia Sleightholme
Email: aess@umich.edu
Phone Number: 7346476004
Principal: N

Name: Levi Theodore Thompson
Email: ltt@umich.edu
Phone Number: 7349362015
Principal: Y

Organization: **University of Michigan - Ann Arbor**
Address: 3003 South State Street, Ann Arbor, MI 481091274
Country: USA

DUNS Number: 073133571 EIN: 386006309
Report Date: 31-Aug-2015 Date Received: 25-Mar-2019
Final Report for Period Beginning 15-Sep-2011 and Ending 31-May-2015
Title: Charge Storage Properties of Early Transition Metal Nitrides
Begin Performance Period: 15-Sep-2011 **End Performance Period:** 31-May-2015
Report Term: 0-Other

Submitted By: Levi Thompson Email: ltt@umich.edu
Phone: (734) 936-2015

Distribution Statement: 1-Approved for public release; distribution is unlimited.

STEM Degrees: 0 **STEM Participants:** 0

Major Goals: To help establish a scientific basis for the design of supercapacitors based on nanostructured early transition metal nitrides by developing relationships between their pseudocapacitive, compositional and structural properties determined under operating conditions where possible.

Accomplishments: High-surface-area nitrides of Ti, V, Nb, Mo, and W were prepared from TiO2 (99.999%, Alfa Aesar), V2O5 (99.999%, Alfa Aesar), Nb2O5 (99.999%, Alfa Aesar), (NH4)6Mo7O24.4H2O (81-83% as MoO3, Alfa Aesar) and WO3
(99.999%, Alfa Aesar) by temperature programmed reaction (TPR) method with
anhydrous NH3 (99.999%, Cryogenic Gases). Figure 1 shows a schematic of the TPR temperature profile. The oxide precursors were first crushed and sieved to retain particles with sizes between 125 and 250 ?m. The particles were supported on a quartz-wool plug in a quartz-tube reactor, which was then loaded into a vertical furnace. After synthesis, the materials were quenched to room
temperature, and then passivated using a flowing mixture of 1% O2/He (99.999%,
Cryogenic Gases) for 5 hours to form an oxygen-rich protective layer that prevents
bulk oxidation of the material when exposed to air.

Training Opportunities: Nothing to Report

Results Dissemination: See attached publications and presentations.

Honors and Awards: Nothing to Report

Protocol Activity Status:

Technology Transfer: Nothing to Report

RPPR Final Report
as of 23-Apr-2019

Charge-Storage Properties of Early Transition Metal Nitrides

Contract: W911NF1110465
Project Final Report May 2015

Project Goal

To help establish a scientific basis for the design of supercapacitors based on nanostructured early transition metal nitrides by developing relationships between their pseudocapacitive, compositional and structural properties determined under operating conditions where possible.

Project Objectives

- Synthesize early transition metal nitride materials with varying surface areas
- Characterize microstructural and compositional properties of the nitride materials using in situ and ex situ methods
- Define key electrochemical properties of the early transition metal nitride materials
- Correlate electrochemical properties with microstructural and compositional properties.

Results

1. Synthesis

High-surface-area nitrides of Ti, V, Nb, Mo, and W were prepared from TiO_2 (99.999%, Alfa Aesar), V_2O_5 (99.999%, Alfa Aesar), Nb_2O_5 (99.999%, Alfa Aesar), $(NH_4)_6Mo_7O_{24}.4H_2O$ (81-83% as MoO_3, Alfa Aesar) and WO_3 (99.999%, Alfa Aesar) by temperature-programmed reaction (TPR) method with anhydrous NH_3 (99.999%, Cryogenic Gases). Figure 1 shows a schematic of the TPR temperature profile. The oxide precursors were first crushed and sieved to retain particles with sizes between 125 and 250 μm. The particles were supported on a quartz-wool plug in a quartz-tube reactor, which was then loaded into a vertical furnace. After synthesis, the materials were quenched to room temperature, and then passivated using a flowing mixture of 1% O_2/He (99.999%, Cryogenic Gases) for 5 hours to form an oxygen-rich protective layer that prevents bulk oxidation of the material when exposed to air. The reaction conditions used to synthesize the nitrides of Ti, V, Nb, Mo, and W metals are listed in Table 1.

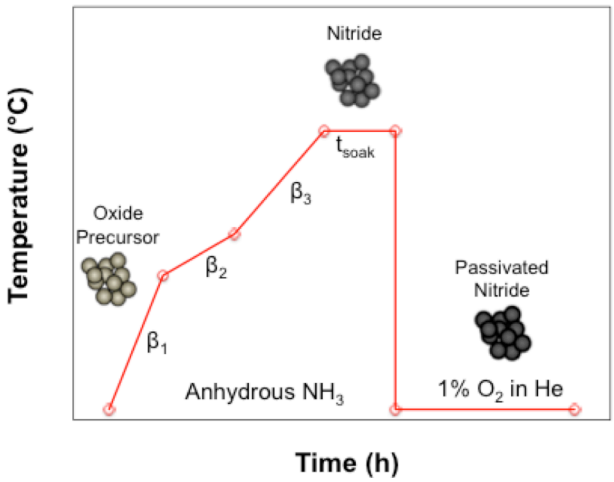

Figure 1. Schematic of the temperature program used to synthesize the nitrides of Ti, V, Nb, Mo, and W metals. β_1, β_2, β_3 represent the heating rates, and t_{soak} is the soak time.

Table 1. Synthesis conditions for high-surface-area Ti, V, Nb, Mo, and W nitrides.

Material	Precursor Weight (g)	Flow rate (mL/min)	T_1 (°C)	β_1 (°C/min)	T_2 (°C)	β_2 (°C/min)	T_3 (°C)	β_3 (°C/min)	t_{soak} (min)
TiN	1.0	450	300	9.2	1000	0.93	-	-	60
VN	0.4	1200	750	5.0	-	-	-	-	60
NbN	1.0	600	800	1.0	-	-	-	-	180
γ-Mo_2N	1.3	400	350	10	450	0.66	700	1.66	120
β-W_2N	1.0	400	350	10.8	460	0.61	750	2.9	60

2. Characterization

Deconvoluting pseudocapacitance and double-layer capacitance. The extent of pseudocapacitance in the nitride-based materials was investigated using cyclic voltammetry and electrochemical impedance spectroscopy (EIS). The pseudocapacitance contribution in all materials was much higher than the double-layer capacitance. The extent of pseudocapacitive charge-storage contribution ranged from 61% for TiN to 84% for VN in acid and base, respectively. The total capacitance of all materials was found to vary logarithmically with scan rate. At lower scan rate, the capacitance reaches a maximum. The number of electrons transferred during pseudocapacitive charge storage was also determined. It was found that there was at least one electron transfer per each material in both acid and base electrolytes.

Cyclic voltammetry was used to determine the total capacitance of each material in both acid and base electrolytes. Table 2 summarizes the surface areas, voltage windows, total capacitance and specific capacitance for phase pure Mo_2N, VN, and TiN in aqueous electrolytes. The surface areas obtained for synthesized materials are similar to those reported in the literature [1,2]. The specific capacitances of all materials are much higher than the expected double-layer capacitances and the specific capacitance of commercial available supercapacitor material (AC295). This indicates pseudocapacitance for these nitride materials. Capacitance and specific capacitance were calculated and plotted as function of scan rate. Figure 2 shows the capacitance as function of scan rate for VN and TiN in 0.1 mol dm^{-3} H_2SO_4 and 0.1 mol dm^{-3} KOH aqueous electrolytes from 2000 mV/s to 2mV/s. The capacitances were logarithmically correlated with scan rate. This is expected for pseudocapacitive materials because of the presence of redox reactions. There were three distinguishable regimes in the plot of capacitance versus scan rate for all materials. At high scan rates (region 1), the capacitance is almost negligible. This is due to the cell resistance and transport limitations occurring at fast scan rates. As the scan rate decreases down to 20 mVs^{-1} (region 2), the capacitance increases significantly. This increase of capacitance with decrease in

Table 2. Physical and electrochemical properties of face-centered cubic nitrides in aqueous media.

Material	Surface Area (m^2g^{-1})	Voltage Window (V)	Gravimetric Capacitance (F/g)	Specific Capacitance (μFcm^{-2})
TiN	18	1.2 (H_2SO_4)	39	217
		1.6 (KOH)	41	228
VN	38	1.1 (H_2SO_4)	171	450
		1.1 (KOH)[1]	210	553
Mo_2N	152	0.8 (H_2SO_4)[1]	346	227
AC295	3261	2.5 (EMImBF4)[2]	350	11

scan rate indicates the ability of electrolyte ions to diffuse into pores. Electrolyte ions have sufficient time to travel the Debye length scale and fill out the pores structures of the materials. This is the regime where the system performance is limited by transport phenomena. At low scan rates (region 3), the plots of capacitance reached a plateau. This region indicates the maximum capacitance of the materials.

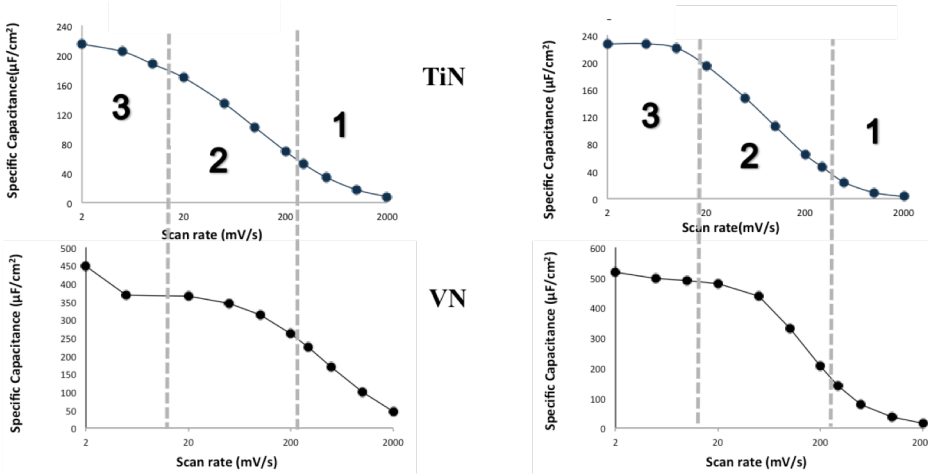

Figure 2. Specific capacitance as function of scan rate for TiN and VN materials in 0.1 M H_2SO_4 (left) and 0.1 M KOH (right).

Electrochemical impedance spectroscopy (EIS) was used to deconvolute the faradaic charge storage (pseudocapacitive) and electrostatic charge storage (double layer) mechanisms of Ti and V based nitride materials in aqueous electrolyes. In EIS, selected potentials within the stable potential window of all materials were modulated using a low amplitude modulation of 10 mV over a wide frequency range from 1 mHz to 100 kHz and the current response of the system was then recorded and evaluated. This allowed us to distinguish the pseudocapacitance and double-layer capacitance of each material in aqueous media. Figure 3 shows plots of capacitance versus the selected potentials.

Surface redox reactions and adsorption of species onto the Ti and V nitride surfaces were indicated by changes in the capacitance at the maximum phase angle. As shown in Figure 3, in the absence of pseudocapacitive charge storage, capacitance goes to a minimal value, indicating only double-layer capacitance. Table 3 summarizes the extent of pseudocapacitance in V, Ti and Mo nitride materials.

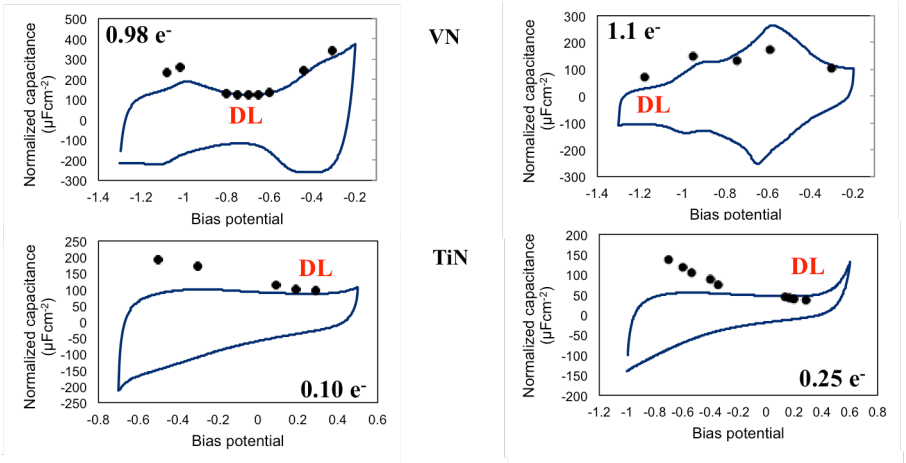

Figure 3. Cyclic voltammograms and normalized capacitance (specific capacitance) calculated from EIS at selected bias potentials within the stable window of TiN and VN materials in 0.1 M H_2SO_4 (left) and 0.1 M KOH (right).

Hydrogen and hydroxide insertion using small angle neutron scattering. Small angle neutron scattering (SANS) technique was used to quantify the amount, depth of storage, and location of hydrogen and hydroxide insertion into the Mo_2N and VN materials, respectively, during

Table 3. Extent of pseudocapacitance in Ti and V nitrides in aqueous media.

Material	Pseudocapacitance (μFcm^{-2})		Pseudocapacitance (%)	
	0.1M H_2SO_4	0.1M KOH	0.1M H_2SO_4	0.1M KOH
VN	307	391	84	79
Mo_2N	137	Unstable	69	Unstable
TiN	132	191	61	84

electrochemical charge storage. SANS experiments were conducted at Oak Ridge National Laboratory (ORNL), using a General Purpose SANS instrument with a neutron wavelength of $\lambda = 4.75$ Å and a wavelength spread, $\Delta\lambda/\lambda$ of 0.13. Two sample-to-detector distances, 12 m and 0.26 m, were used to cover a Q range between 0.001 $Å^{-1}$ to 1.0 $Å^{-1}$, where Q is the scattering vector. Average acquisition time for each scattering curve was approximately 30 min. Scattering patterns were corrected for instrumental background, transmission and detector efficiency. The raw 2D data were reduced to 1D profile, I (Q) versus Q. The data were placed on an absolute scale (cm^{-1}) using pre-calibrated standards. The measurements were conducted at room temperature. SANS patterns were first recorded from dry Mo_2N and VN electrodes. After, approximately 10 ml of 0.1 mol dm^{-3} H_2SO_4 in D_2O and 0.1 mol dm^{-3} KOH in D_2O solutions were added to the Mo_2N and VN systems, respectively, and SANS spectra were collected at different applied voltages to monitor the changes in the distribution of hydrogen and hydroxide ions as function of applied potentials and pore sizes. The Beaucage model was used to deconvolute scattering intensities from pores of different sizes.

For the Mo_2N material, the moles of inserted hydrogen and electron transferred as function of applied potentials are shown in Figure 4a. Both, varied significantly with potentials, and followed similar trend suggesting that during electrochemical charge storage, H^+ and e^- are simultaneously inserted into Mo_2N. To better understand the charge process in the Mo_2N material, ratios of moles of H^+ to e^- and H^+ to Mo_2N have been plotted (Figure 4b). The H^+/e^- ratio increases as high as 0.5 as the potential was increased from left to right, indicating insertion of $1H^+$ per $2e^-$. For a given electrochemical reaction, the charge is always balanced as dictated by charge neutrality. Therefore, for the insertion of $1H^+$ per $2e^-$, the Mo metal in the Mo_2N must be reduced. Recently, we have demonstrated, using X-ray absorption spectroscopy, addition of 1e- per Mo, during electrochemical charge

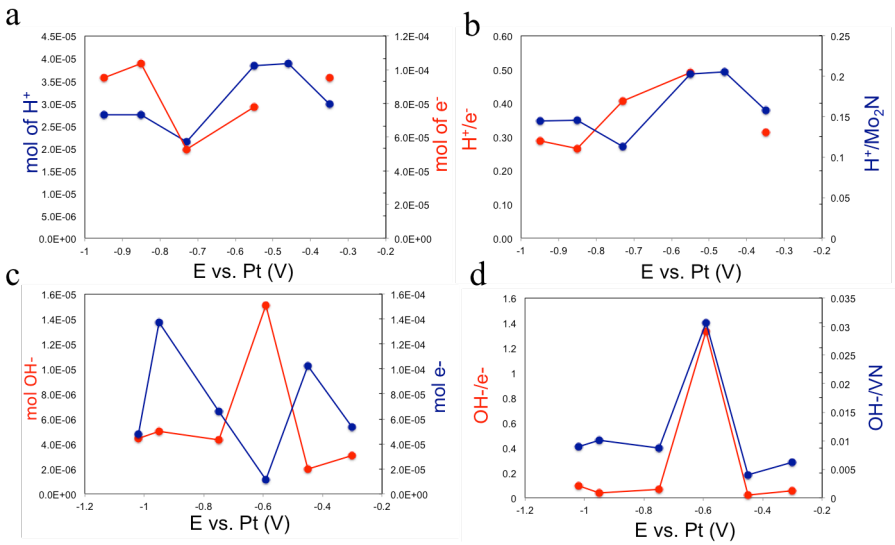

Figure 4. Moles of hydrogen (blue) and mole of electron transferred (red) for Mo_2N (a), ratio of hydrogen over electron (red) and ratio of hydrogen over Mo_2N material (b) in 0.1M H_2SO_4 in D_2O; mole of hydroxide (red) and mole of electron transferred (blue) for VN (c) , ratio of hydroxide over electron (red) and ratio of hydroxide over VN material (d) in 0.1M KOH in D_2O.

storage. This is consistent with our findings, both indicating $1e^-$ transfer per Mo or $2e^-$ transfer per $1H^+$, as the material was cycled within its stability window. Combining results from physical, electrochemical, surface, and bulk characterizations, we propose the following reaction for Mo_2N during charge storage in aqueous acidic media:

$$Mo_2{}^{\alpha}N + 2H^+ + 4e^- \leftrightarrow Mo_2{}^{\alpha-1}N(H)_2$$

For the VN material in basic media, the moles of extracted hydroxide and electron transferred as function of applied potentials are shown in Figure 4c. Unlike the process in the Mo_2N material, moles of hydroxide and moles of electron followed opposite trend suggesting that during electrochemical charge storage, OH^- and e^- are on opposite sites of the redox reaction. Figure 4d shows ratios of moles of OH^- to e^- and OH^- to VN material. As the material was cycled, OH^-/e^- ratio increases as high as close to 2, suggesting storage of $2OH^-$ per $1e^-$. Considering all of the results, we proposed the following reaction mechanism for VN in basic media, in which application of an electric field induces desorption/extraction of OH^- in the VN material.

$$V^{\alpha}N + 2OH^- \leftrightarrow V^{\alpha-1}N(OH)_2 + e^-$$

To get insight about the distribution and location of hydrogen and hydroxide ions in the pores of Mo_2N and VN materials, respectively, the Beaucage model was used to decouple the contribution of hydrogen and hydroxide adsorption and desorption into macropores (>50 nm), mesopores (2-50 nm), and micropores (<2 nm). Figures 5a and 5b show the density of hydrogen insertion in pores and hydroxide desorption from pores of the Mo_2N and VN, respectively. Additionally, in the VN system, we replaced OH^- ions by OD^- ions, to track the effects of contrast matching and isotope labeling on the charge storage process (Figure 5b).

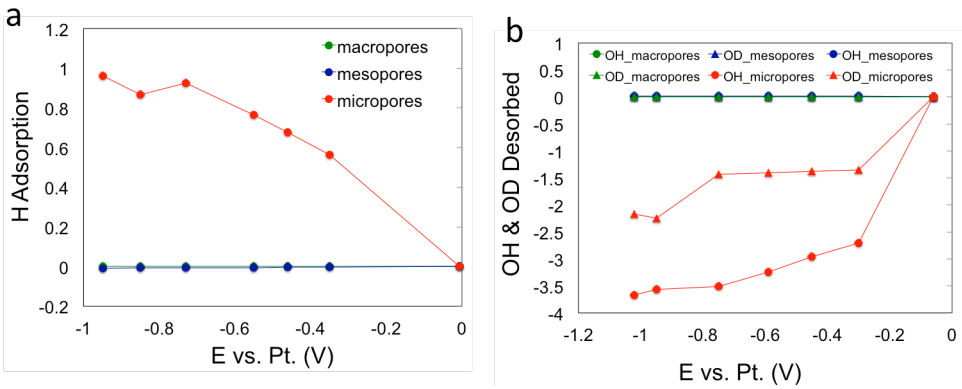

Figure 5. Density of hydrogen distribution in the pores of Mo_2N (a) and density of hydroxide distribution in VN (b), as function of applied potentials.

For the Mo_2N material, in pores of 2 nm size (border limit between mesopores and micropores), the density of hydrogen insertion significantly increases as the potential was expanded from an open circuit potential (at one end of the voltage window) to the other end of the voltage window. There was minimal adsorption of hydrogen in the large pores (mesopores and macropores). Similar trend was found in the VN system. Upon application of an electric field, desorption of hydroxide ions significantly increased in pores of 2 nm sizes than any other pores sizes. Deuterium system followed similar trend, as expected. Additionally, the intensity

decreased when switching OH^- to OD^-, indicating the effect of isotope and contrast matching on the charge storage process.

Ultimately, these results will not only benefit efforts to develop high-energy supercapacitors based on early transition metal nitrides but also enhance our understanding of characteristics contributing to their electrocatalytic and catalytic properties.

3. Correlating Electrochemical Properties with Microstructural and Compositional Properties

Effects of Passivation on Nitrides. Physical and electrochemical properties of passivated (thin oxide layer on the surface) and unpassivated materials was determined using physical and electrochemical characterization techniques including N_2 physisorption and cyclic voltammetry, respectively. Surface areas for selected passivated and unpassivated nitrides are listed in Table 4.

Table 4. Surface areas for selected passivated and unpassivated nitride materials.

Material	Surface Areas (m^2g^{-1})	
	Passivated	Unpassivated
VN	34	33
TiN	18	20
W_2N	68	67
Mo_2N	136	169

There was increase in the surface areas observed for only Mo_2N material. However, considerable differences were observed in the pore sizes distributions for most materials (Figure 6). The Mo_2N material showed increased in the pore volume, consistent with the observed surface area. The pore size distribution for the unpassivated VN material shifted to smaller pore sizes relative to that for the passivated material. Passivated and unpassivated TiN and W_2N materials showed similar pore sizes distribution.

The correlation of areal specific capacitance with scan rate for all selected materials are shown in

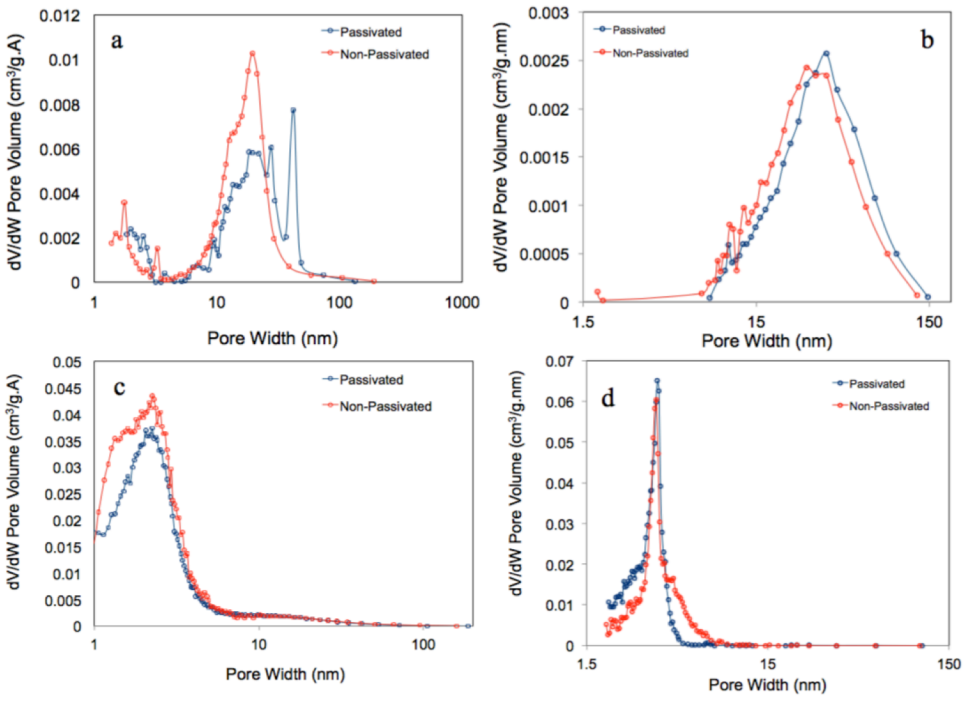

Figure 6. Pore size distributions for passivated (blue) and unpassivated (red) of VN (a), TiN (b), Mo_2N (c) and W_2N (d) nitrides.

Figures 7 and 8 in aqueous acidic and basic electrolytes, respectively. The specific capacitances for unpassivated materials were slightly higher at lower scan rate compared to those for passivated materials, indicating improved pseudocapacitive storage in unpassivated materials. From N_2 physisorption analysis, in comparison to passivated materials, unpassivated materials exhibited higher density of micropores, which are the most active for pseudocapacitive charge storage as indicated by results from *In-situ* small angle neutron scattering analysis. It is believed that the moderate improvement in performance owns to the absence of oxide thin layer on the unpassivated materials.

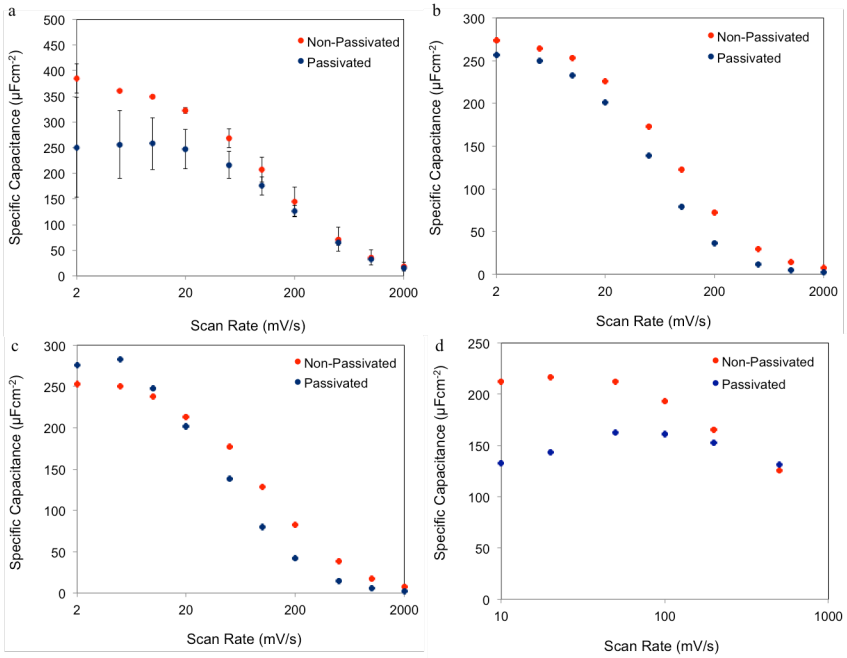

Figure 7. Specific capacitance as function of scan rate for VN (a), W_2N (b), Mo_2N (c), and TiN (d) in 0.1 mol dm^{-3} H_2SO_4 electrolyte.

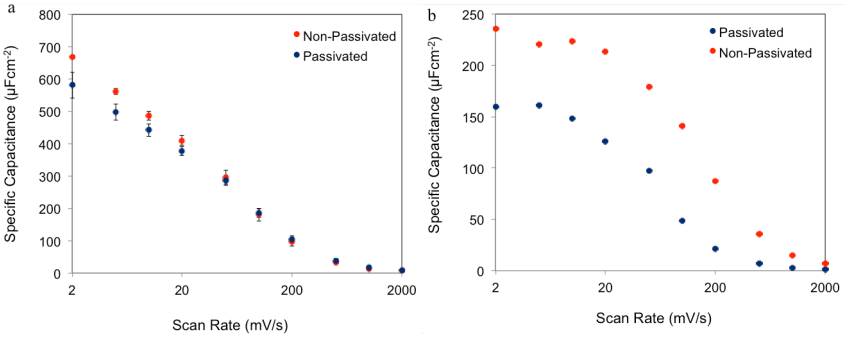

Figure 8. Specific capacitance as function of scan rate for VN (a) and W_2N (b) in 0.1 mol dm^{-3} KOH electrolyte.

Effects of crystallite structure and composition on charge storage. A series of nanostructured Ti, V, Nb, Mo, and W interstitial compounds nitrides and carbides were synthesized using a temperature-program reaction method. Physical properties for all synthesized materials are listed in Table 5.

The materials were found to be electrochemically stable in both aqueous KOH and H_2SO_4 electrolytes. All materials except β-W_2N in basic electrolyte, NbC and VC in acidic electrolyte showed high areal specific capacitance exceeding double layer charging, suggesting charge storage contributions from a pseudocapacitive mechanism. The capacitances of all studied materials were found to vary logarithmically with scan rate and reach a maximum value at a lower scan rate (2 mV/s), which indicated the contribution to charge storage from a pseudocapacitive storage mechanism (Figure 8). The effect of crystalline structure, type of metals, and non-metals on the pseudocapacitive charge storage was further investigated. In basic electrolyte, the pseudocapacitive charge storage for fcc structured Mo carbides was higher than those for hcp-based structured Mo carbide materials, whereas, in acidic electrolyte, hcp-based structures exhibited the highest pseudocapacitance. The nitride-based materials that have 1:1

metal to non-metal stoichiometry exhibited higher pseudocapacitance than those with 2:1 stoichiometry due to the electroactive interaction of nitrogen with H^+ and OH^- (Figure 9). Conversely, the carbide-based materials that have 2:1 stoichiometry exhibited higher pseudocapacitance than those with 1:1 stoichiometry partly due to undesirable interaction of carbon with oxygen, but mostly due to their higher density of interstices. Ultimately, these findings serve as useful correlation and prediction tools for the electrochemical, electrocatalytic, and catalytic performance of interstitial compounds nitrides and carbides, and are of interest in the design of higher-energy-density nitride and carbide-based supercapacitor electrode materials.

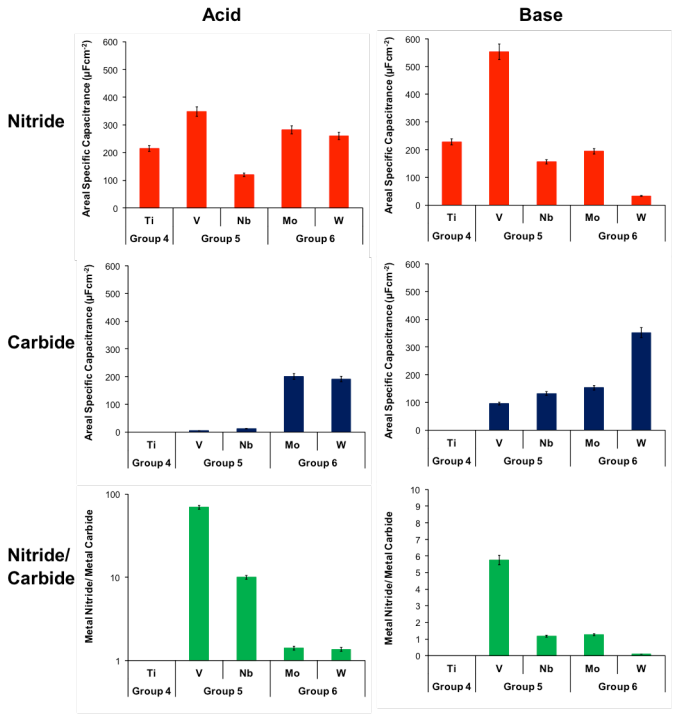

Figure 9. Clustered bar chart of total areal specific capacitance as a function of composition for fcc structures early transition metal nitrides (red) and carbides (blue), and ratio of the areal specific capacitance of the nitrides over carbides of the same metal (green), in aqueous media.

Table 5. Physical properties of early transition-metal carbides and nitrides.

Material	Electrical Conductivity (Sm^{-1}) x 10^7	Interstices/Mole Material (x 10^{21})	Crystallite Size (nm)	Surface Area (m^2g^{-1})	Pore Volume (cm^3g^{-1})	Micropore Volume (cm^3g^{-1})
TiN[a]	0.40	1.20	15	18	0.20	0.008
VN[a]	0.12	1.21	21	32	0.18	0.02
VC[a]	0.16	1.20	14	6	0.03	0.0004
NbN[a]	0.17	1.20	13	34	0.06	0.021
NbC[a]	0.29	1.20	15	16	0.05	0.01
β-W_2N[b]	1.11	3.01	6.0	42	0.02	0.03
β-WC_{1-x}[b]	0.45	2.92	6.0	65	0.07	0.053
γ-Mo_2N[b]	0.51	3.01	6.0	144	0.12	0.08
α-Mo_2C[b]	-	3.01	6.0	92	0.16	0.003
β-Mo_2C[c]	0.14	0.36	6.0	82	0.13	0.007
(α+β)-Mo_2C[d]	-	-	-	88	0.14	0.009

Products of Research

Journal Articles

1. A. Djire, O.T. Ajenifujah, A.E.S. Sleightholme, P.G. Rasmussen and L.T. Thompson, "Effects of Surface Oxygen on Charge Storage in High Surface Area Early Transition-Metal Carbides and Nitrides," J. Power Sources **207** (2015) 159-166.
2. P. Pande, A.E.S. Sleightholme, P. Rasmussen, A. Deb, J. Penner-Hahn and L.T. Thompson, "In Situ Characterization of Molybdenum Nitride Supercapacitor Electrodes," J. Power Sources **289** (2015) 154-159.
3. A. Djire, O.T. Ajenifujah, A.E.S. Sleightholme, P.G. Rasmussen, S. Choi and L.T. Thompson, "Extent of Pseudocapacitance in Early Transition Metal Carbides and Nitrides," in preparation for submission to J. Mat. Chem. A.
4. A. Djire, O.T. Ajenifujah, A.E.S. Sleightholme, S. Choi, P. Rasmussen and L.T. Thompson, "Effects of Crystal Structure and Composition on the Charge Storage Properties of Early Transition-Metal Nitrides and Carbides," in preparation for submission to J. Mat. Chem. A.
5. A. Djire, A.E.S. Sleightholme, J.B. Siegel and L.T. Thompson, "Extent of Pseudocapacitance in Early Transition-Metal Carbides and Nitrides," in preparation for submission to J. Electrochem. Soc.
6. A. Djire, J.B. Siegel, L. He and L.T. Thompson, "Pseudocapacitive Hydrogen Storage in High-Surface Area Molybdenum Nitrides," in preparation for submission to J. Amer. Chem. Soc.

Conference Presentations

1. A. Djire, P. Pande, A. Deb, A. Sleightholme, P. Rasmussen, J. Penner-Hahn and L. Thompson, "Pretreatment Effects on Charge Storage of Early Transition-metal Carbides and Nitrides," AIChE Meeting, November 2013, San Francisco, USA.
2. A. Djire, P. Pande, A. Deb, A. Sleightholme, P. Rasmussen, J. Penner-Hahn and L. Thompson, "Pretreatment Effects on Charge Storage of Early Transition-metal Carbides and Nitrides," 224th Electrochemical Society Meeting, November 2013, San Francisco, USA.
3. A. Djire, O.T. Ajenifujah, A. Sleightholme, P. Rasmussen and L. Thompson, "Double-Layer and Pseudocapacitive Charge-Storage Mechanisms in Carbides and Nitrides," Power Sources Meeting, June 2014, Florida, USA.
4. A. Djire, O.T. Ajenifujah, A.E. Sleightholme, P. Rasmussen and L.T. Thompson, " Double-Layer and Pseudocapacitive Charge Storage Mechanism in Carbides and Nitrides," ECS Annual Meeting, Cancun, Mexico, October, 2014.
5. A. Djire, O.T. Ajenifujah, A.E. Sleightholme, P. Rasmussen and L.T. Thompson, "Double-Layer and Pseudocapacitive Charge Storage Mechanism in Carbides and Nitrides," AIChE Annual Meeting, Atlanta, GA, November, 2014.
6. A. Djire, O.T. Ajenifujah, A.E. Sleightholme, J. Siegel, L. He, P. Rasmussen and L.T. Thompson, "Charge Storage Mechanism of Carbides and Nitrides," ECS Annual Meeting, Chicago, IL, May, 2015.
7. A. Djire, J. Siegel, Lilin He, A.E. Sleightholme, S. Choi, P. Rasmussen and L.T. Thompson, "Charge Storage Mechanism for High Surface Areas Carbides and Nitrides," AIChE Annual Meeting, Salt Lake City, UT, November, 2015, submitted.